

# Effects of bone- and air-tissue inhomogeneities on the dose distributions of the Leksell Gamma Knife<sup>®</sup> calculated with PENELOPE

Feras M.O. Al-Dweri<sup>1</sup>, E. Leticia Rojas<sup>1,2</sup> and Antonio M. Lallena<sup>1</sup>

<sup>1</sup> Departamento de Física Moderna, Universidad de Granada, E-18071 Granada, Spain.

<sup>2</sup> Instituto Nacional de Investigaciones Nucleares, Carretera México-Toluca, km 36.5, Ocoyoacac, C.P. 52045, México.

Monte Carlo simulation with PENELOPE (v. 2003) is applied to calculate Leksell Gamma Knife<sup>®</sup> dose distributions for heterogeneous phantoms. The usual spherical water phantom is modified with a spherical bone shell simulating the skull and an air-filled cube simulating the frontal or maxillary sinuses. Different simulations of the 201 source configuration of the Gamma Knife have been carried out with a simplified model of the geometry of the source channel of the Gamma Knife recently tested for both single source and multisource configurations. The dose distributions determined for heterogeneous phantoms including the bone- and/or air-tissue interfaces show non negligible differences with respect to those calculated for a homogeneous one, mainly when the Gamma Knife isocenter approaches the separation surfaces. Our findings confirm an important underdosage ( $\sim 10\%$ ) nearby the air-tissue interface, in accordance with previous results obtained with PENELOPE code with a procedure different to ours. On the other hand, the presence of the spherical shell simulating the skull produces a few percent underdosage at the isocenter wherever it is situated.

## 1. Introduction

GammaPlan<sup>®</sup> (GP) (Elekta 1996) is a computer-based treatment dose planning system designed to calculate the dose distributions of the Leksell GammaKnife<sup>®</sup> (GK) for stereotactic radiosurgery of certain brain diseases. As almost all radiosurgery planning systems, GP is quite simplistic. Using a standard set of beam data, the dose distributions in patients are calculated by adding those corresponding to each one of the 201 beams of the GK actually present in each particular treatment (Wu *et al* 1990, Wu 1992). GP assumes homogeneous target media and tissue heterogeneities are not taken into account (Yu and Sheppard 2003).

However, in stereotactic radiosurgery, Solberg *et al* (1998) have pointed out a remarkable disagreement between Monte Carlo (MC) results and those predicted by the usual planning systems, in case inhomogeneous phantoms are considered.

In the investigation of dose perturbations produced by heterogeneities, MC has showed up as a useful tool, mainly because it accounts, in an adequate way, for the lack of electron equilibrium near interfaces. For the GK, Cheung *et al* (2001), using the EGS4 MC code, have found discrepancies up to 25% in case of extreme irradiation conditions, mainly near tissue interfaces and dose edges. This contrasts with the sub-millimeter accuracy with which GK operates (Elekta 1992).

In this paper we have investigated the effects of bone- and air-tissue interfaces on dosimetric calculations involving the GK. To simulate the GK, a simplified geometry model of the source channels is considered to perform the calculations. This model was proposed in Al-Dweri *et al* (2004) and it is based onto the characteristics shown by the beams after they pass through the treatment helmets. It has been shown that the collimation system of each source channel acts as a “mathematical collimator” in which a point source, situated at the center of the active core of the GK source, emits photons inside the cone defined by



simplified geometry model which is described in detail in Al-Dweri *et al* (2004). It consists of a point source emitting the initial photons in the cone defined by source itself and the helmet outer collimators. The coordinates of the 201 point sources can be found in Al-Dweri and Lallena (2004). They are distributed in the  $z < 0$  region and correspond to the situation in which the isocenter of the GK coincides with the center of the phantom. For the simulations described below, in which the isocenter is situated at different positions, these coordinates must be shifted. The position of the isocenter appears explicitly in the figures as  $I[x_I, y_I, z_I]$ , with the values of the coordinates in mm.

Due to the fact that the distribution of the sources is not completely uniform, no cylindrical symmetry is shown by the system. Thus, the doses we have calculated depend on the three cartesian coordinates,  $D^{(m_1 m_2)}(x, y, z)$ . The superscript refers to the materials of the particular phantom  $\mathcal{P}_{m_1 m_2}$  considered in the simulation. Throughout the paper, the values of the coordinates are given in mm.

Cheung *et al* (2001) used a phantom similar to our  $\mathcal{P}_{wb}$ . It included the 5 mm width bone shell at 5 mm of the phantom surface as in our case, but with a full diameter of 180 mm. This phantom cannot be positioned inside the treatment helmets in such a way that the isocenter of the GK approaches the skull interface. That is why in our simulations we have chosen the phantom described above, which is slightly smaller. In any case, we have compared our results with those of Cheung *et al* by performing simulations with their phantom, which we label  $\overline{\mathcal{P}}_{wb}$ . To do that we have calculated the quantity

$$D_{\text{norm}}(x, y, z) = \frac{D^{(wb)}(x, y, z)}{[D^{(wb)}(x, y, z)]_{\text{max}}}, \quad (1)$$

which corresponds to the dose obtained for  $\overline{\mathcal{P}}_{wb}$  divided by its maximum.

A first evaluation of the effects of the different interfaces has been obtained by calculating the relative differences

$$\Delta_{\text{ww}}^{(m_1 m_2)}(x_I, y_I, z_I) = \frac{D^{(m_1 m_2)}(x_I, y_I, z_I) - D^{(ww)}(x_I, y_I, z_I)}{D^{(ww)}(x_I, y_I, z_I)} \quad (2)$$

between the doses obtained at the isocenter for the heterogeneous,  $\mathcal{P}_{m_1 m_2}$ , and homogeneous,  $\mathcal{P}_{ww}$ , phantoms.

In addition, we have calculated the quantity

$$d_{\text{ww}}^{(m_1 m_2)}(x, y, z) = \frac{D^{(m_1 m_2)}(x, y, z)}{[D^{(ww)}(x, y, z)]_{\text{max}}}, \quad (3)$$

in order to analyze the differences observed in the dose profiles calculated for the different phantoms.

## 2.2. Monte Carlo calculations

PENELOPE (v. 2003) (Salvat *et al* 2003) has been the MC code used to perform the calculations. PENELOPE permits the simulation of the coupled transport of electrons and photons, for an energy range from a few hundred eV up to 1 GeV, for arbitrary materials. PENELOPE provides an accurate description of the particle transport near interfaces.

Photons are simulated in PENELOPE in a detailed way. Electrons and positrons are simulated by means of a mixed scheme which includes two types of events: hard events, which are simulated in detail and are characterized by polar angular deflections or energy losses larger than certain cutoff values, and soft events, which are described in terms of a condensed simulation based on a multiple scattering theory (Salvat *et al* 2003). The tracking

**Table 1.** PENELOPE tracking parameters of the materials assumed in our simulations.  $E_{\text{abs}}(\gamma)$  and  $E_{\text{abs}}(e^-, e^+)$  stand for the absorption energies corresponding to photons and electrons and positrons, respectively.

materials	Air	Bone and Water
$E_{\text{abs}}(\gamma)$ [keV]	1.0	1.0
$E_{\text{abs}}(e^-, e^+)$ [keV]	0.1	50.0
$C_1$	0.05	0.1
$C_2$	0.05	0.05
$W_{\text{cc}}$ [keV]	5.0	5.0
$W_{\text{cr}}$ [keV]	1.0	1.0
$s_{\text{max}}$ [cm]	$10^{35}$	$10^{35}$

**Table 2.** Composition of the materials assumed in the MC simulations performed in this work. The values correspond to the weight fraction of each element in the material. Also the densities are quoted. The three materials have been generated with the code `material` included in the PENELOPE package and correspond to the numbers 104, 119 and 277 respectively in the material database of the MC code.

	Air	Bone	Water
H		0.52790	0.111894
C	0.000124	0.19247	
N	0.755267	0.01603	
O	0.231781	0.21311	0.888106
Mg		0.00068	
P		0.01879	
S		0.00052	
Ar	0.012827		
Ca		0.03050	
density [g cm <sup>-3</sup> ]	0.0012048	1.85	1.0

is controlled by means of the four parameters  $C_1$ ,  $C_2$ ,  $W_{\text{cc}}$  and  $W_{\text{cr}}$ , as well as the absorption energies. All these parameters must be fixed for the materials present in the geometry considered in the simulation. Table 1 shows the values we have assumed in our simulations. In addition we have fixed the parameter  $s_{\text{max}} = 10^{35}$  in all the simulations performed.

The initial source was selected by sampling uniformly between the 201 sources. Initial photons were emitted with the average energy 1.25 MeV and uniformly in the corresponding emission cone.

The simulation geometry has been described by means of the geometrical package PENGEOm of PENELOPE. The three materials assumed in the simulations performed (air, bone and water) have been generated with the code `material` included in the PENELOPE package. Table 2 gives the composition and densities of these materials.

To score the doses we have considered cubic voxels with  $\Delta x = \Delta y = \Delta z = 1$  mm, for the 18 and 14 mm helmets, and  $\Delta x = \Delta y = \Delta z = 0.5$  mm, for the 8 and 4 mm ones. In the calculation of the doses  $D^{(m_1 m_2)}(x_I, y_I, z_I)$ , used to determine the relative differences  $\Delta_{\text{ww}}^{(m_1 m_2)}(x_I, y_I, z_I)$  as given by equation (2), voxels with double width in the  $y$  direction were

considered.

The number of histories followed in each simulation has been  $3 \cdot 10^8$ . This permitted to maintain the statistical uncertainties under reasonable levels. The uncertainties given throughout the paper correspond to  $1\sigma$ . In much of the figures, the error bars do not show up because they are smaller than the symbols used.

### 3. Results

#### 3.1. Comparison with EGS4 calculations

First of all we have compared our results with those obtained by Cheung *et al* (2001) using the EGS4 code. They considered the 18 mm helmet for two situations of the isocenter: I[0,-66,0] and I[0,0,-69]. Their results (solid curves) are compared with our findings (open squares) in figure 2, where the values of  $D_{\text{norm}}(x, y, z)$ , as given by equation (1), are plotted for the three cartesian axes and the two positions of the isocenter. As we can see, both calculations are in good agreement for the two cases considered.

In the figure, also the predictions of the GP, quoted by Cheung *et al* (2001), are included (dashed curves). For the isocenter at I[0,-66,0], a discrepancy between MC simulations and GP results is observed in the far negative  $y$  region (see medium left panel). This is due to the fact that the GP does not take into account the interfaces and assumes all tissue to be uniformly represented by water. The same situation is not observed when the isocenter is at I[0,0,-69] (see right lower panel), because in that case the dose is roughly zero before reaching the interface (for  $z \sim -80$  mm).

#### 3.2. Comparison with GammaPlan predictions

Figure 3 shows a comparison of different simulations performed for the phantom  $\overline{\mathcal{P}}_{\text{ww}}$  (open squares) with GP predictions of Hamad and Mherat (2005) (dashed curves). In the upper panels the isocenter is situated at I[0,34,0] and the profiles along  $y$  axis are shown for the 18 and 4 mm helmets. The isocenter situated at I[0,66,0] in medium panels where the profiles along  $x$  and  $z$  axes are shown for the 14 mm helmet. Finally, the profiles along  $y$  axis are shown in lower panels, for the 14 and 8 mm helmets and the isocenter situated at I[0,70,0].

As we can see, the simulation for the water phantom produces results in very good agreement with the GP predictions. Below (see section 3.4), the effects of the interfaces in these cases will be analyzed and it will be clear that GP cannot describe these effects.

This is evident also in right tail of the profiles shown in the lower panels. We can see how a clear discrepancy between the simulation and the GP appears at  $y = 80$  mm, that is, at the external border of the phantom. There in, an interface air-water is considered in the simulation, while GP does not take into account such a situation.

#### 3.3. Effects of the tissue inhomogeneities on dose at the isocenter

Now we analyze the results obtained for different positions of the isocenter of the GK, paying special attention to the situations in which the isocenter is close to the interfaces.

First, we have investigated the effects of tissue inhomogeneities on the doses calculated at the isocenter. We have varied its position by fixing the coordinate  $y_I$  at different values ranging from -70 mm to 70 mm and maintaining  $x_I = z_I = 0$ . The results obtained for the relative differences with respect to the homogeneous phantom,  $\Delta_{\text{ww}}^{(m_1, m_2)}(0, y_I, 0)$ , as given by equation (2), are shown in figure 4. Therein, upper panels correspond to the phantom  $\mathcal{P}_{\text{wb}}$ ;

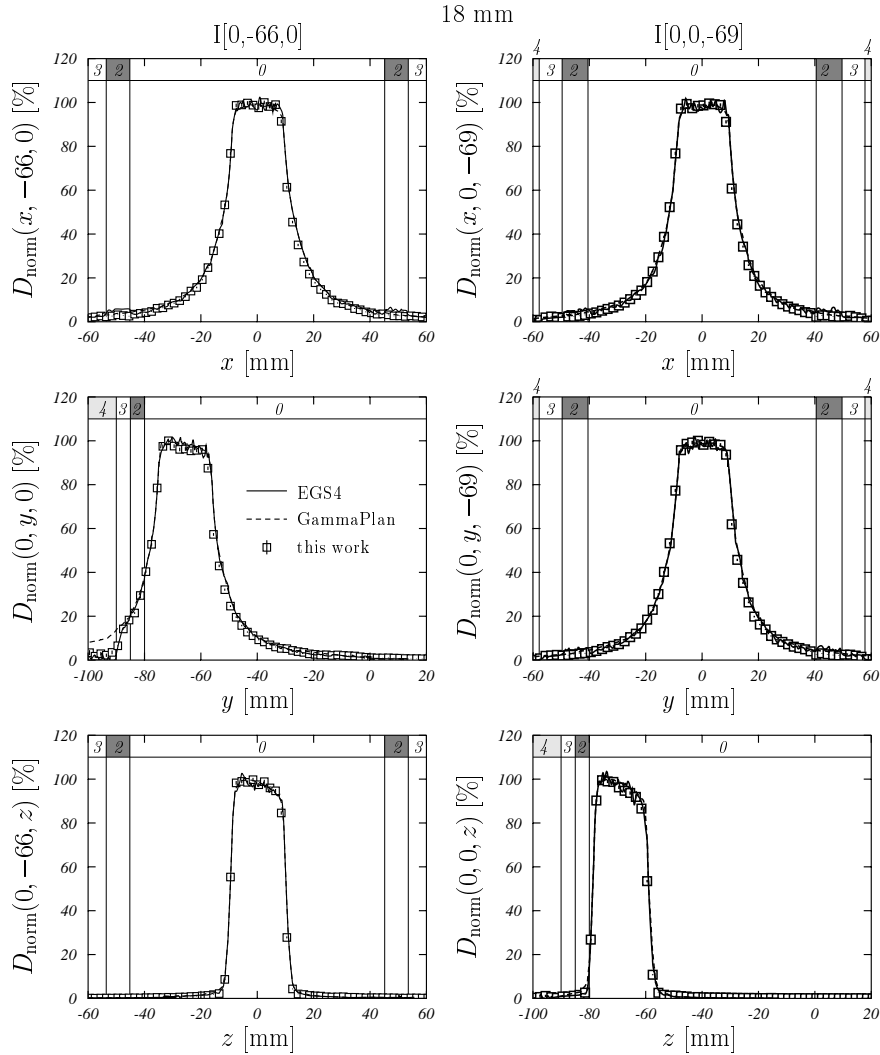


**Figure 2.** Dose profiles at the isocenter, relative to their respective maxima, in percentage, for the 18 mm helmet. Panels show the results along  $x$  (upper),  $y$  (medium) and  $z$  (lower) axes. Left panels correspond to the isocenter situated at  $I[0, -66, 0]$ , while in the right panels the isocenter is at  $I[0, 0, -69]$ . Open squares are the results of our simulations. Full curves correspond to EGS4 results quoted Cheung *et al* (2001). Dashed curves correspond to the predictions of GP quoted by the same authors. The phantom  $\overline{\mathcal{P}}_{wb}$  has been considered in this case.

medium panels represent the results in case of the heterogeneous phantom  $\mathcal{P}_{aw}$ , and, finally, in the lower panels the phantom  $\mathcal{P}_{ab}$  has been considered. We have plotted the results for the 18 mm (left panels) and 8 mm (right panels) helmets. Similar results are obtained for the 14 and 4 mm helmets.

As we can see, the presence of the bone spherical shell (upper panels) produces a reduction of the dose at the isocenter with respect to that obtained for the homogeneous phantom. This reduction is observed at practically any position of the isocenter, being  $\sim 3\%$  for the two helmets. A higher perturbation in the dose is observed when the isocenter is situated exactly at the interface bone-water,  $y_I = \pm 70$  mm. In this case, the reduction in the dose rises to 5% for the 18 mm helmet and it is even larger for the 8 mm one. It seems

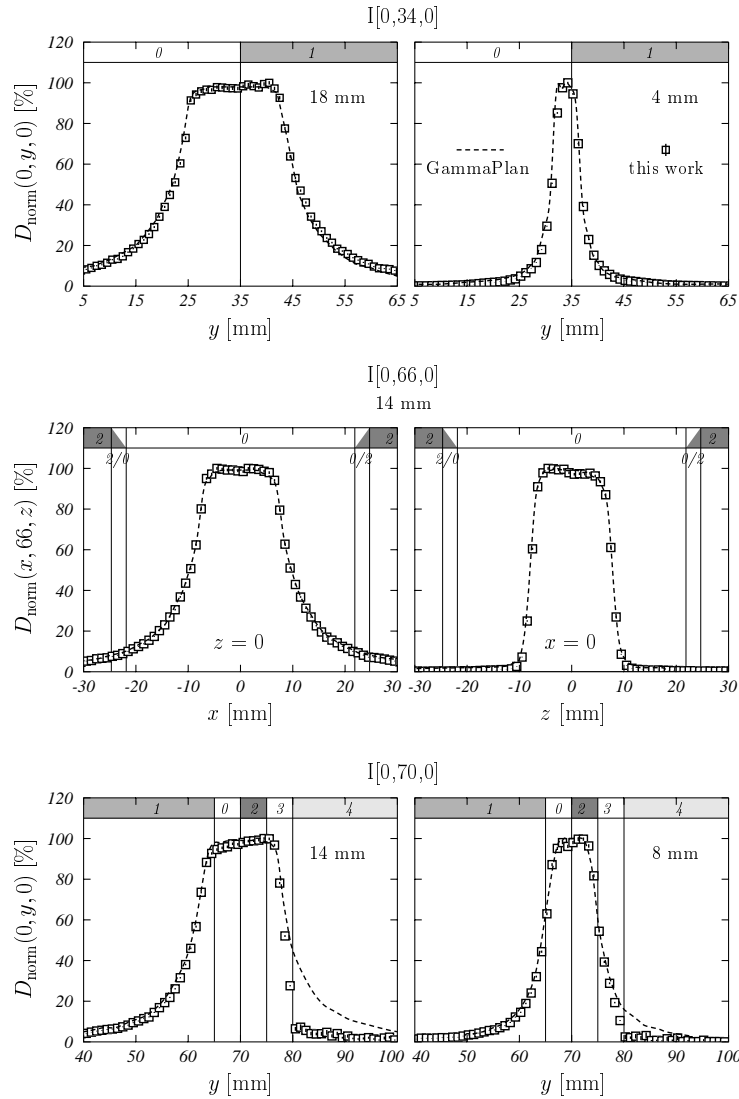


**Figure 3.** Dose profiles at the isocenter, relative to their respective maxima, in percentage, for different positions of the isocenter. Open squares are the results of our simulations performed with the phantom  $\overline{\mathcal{P}}_{\text{ww}}$ . Dashed curves are GammaPlan predictions (Hamad and Mherat, 2005). Upper panels correspond to the isocenter situated at I[0,34,0] and show the profiles along  $y$  axis for the 18 and 4 mm helmets. Medium panels show the profiles along  $x$  (left) and  $z$  (right) axes for the 14 mm helmet with the isocenter situated at I[0,66,0]. Lower panels are similar to the upper ones but for the isocenter situated at I[0,70,0] and for the 14 and 8 mm helmets.

evident from our results that the effect of the full skull, which we simulate here by means of the bone spherical shell, is not negligible at all.

To have an idea about the origin of this effect, we have evaluated the reduction in the dose due to the bone inhomogeneity in a very simple case. We have considered a photon pencil beam coming from the source and reaching the phantom and we have calculated the dose at the isocenter neglecting scattering photons. In case the phantom  $\mathcal{P}_{\text{wb}}$  is considered, the dose at the isocenter is proportional to (see e.g. Berger, 1968)

$$D^{(\text{wb})}(x_I, y_I, z_I) \propto \left( \frac{\mu_{\text{en}}}{\rho} \right)_{\text{w}} \frac{E_0}{4\pi r^2} \exp[-\mu_{\text{a}}s_4 - \mu_{\text{w}}s_3 - \mu_{\text{b}}s_2 - \mu_{\text{w}}s_0], \quad (4)$$

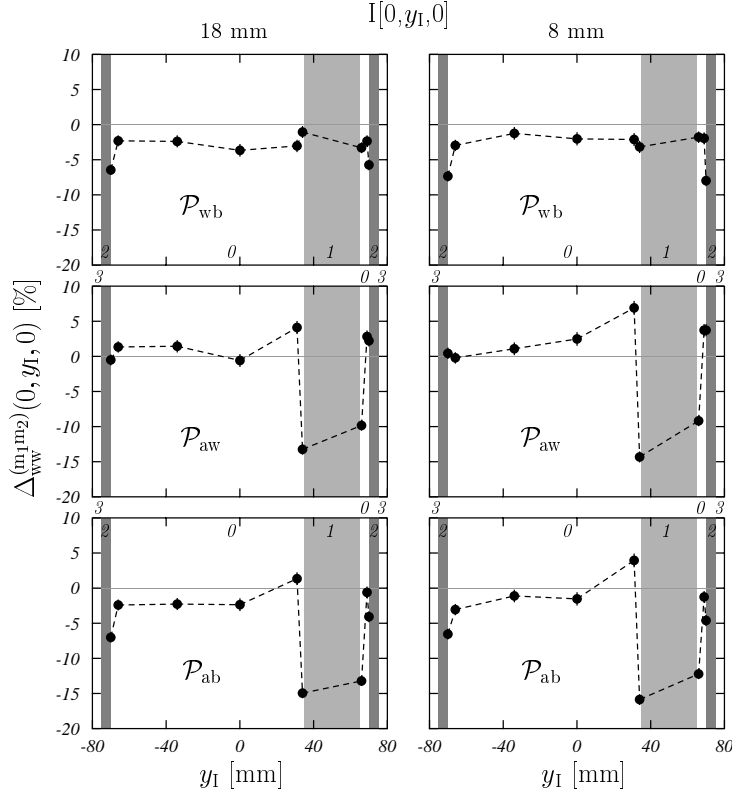


**Figure 4.** Relative differences  $\Delta_{\text{ww}}^{(\text{m}_1\text{m}_2)}(0, y_I, 0)$  in percentage, between the doses calculated at the isocenter for heterogeneous and homogeneous phantoms (see equation (2)). Upper panel corresponds to the phantom  $\mathcal{P}_{\text{wb}}$ ; medium panel represents the results in case the heterogeneous phantom  $\mathcal{P}_{\text{aw}}$ , and in the lower panels the phantom  $\mathcal{P}_{\text{ab}}$  has been considered. Results for the 18 mm (left panels) and 8 mm (right panels) helmets are shown.

where  $(\mu_{\text{en}}/\rho)_{\text{w}}$  is the mass energy absorption coefficient of water at the initial energy of the photons,  $E_0$ , and  $\mu_{\text{a}}$ ,  $\mu_{\text{w}}$  and  $\mu_{\text{b}}$  are the attenuation coefficients of air, water and bone, respectively, at the same energy. The values  $s_i$  correspond to the length of the trajectory segments traveled in the region  $i$  of the phantom and thus,

$$r = s_4 + s_3 + s_2 + s_0 \quad (5)$$

is the distance from the source to the isocenter. If we consider the phantom  $\mathcal{P}_{\text{ww}}$ ,

$$D^{(\text{ww})}(x_I, y_I, z_I) \propto \left( \frac{\mu_{\text{en}}}{\rho} \right)_{\text{w}} \frac{E_0}{4\pi r^2} \exp[-\mu_{\text{a}}s_4 - \mu_{\text{w}}(s_3 + s_2 + s_0)]. \quad (6)$$

We are interested in the fraction of both doses, which is given by

$$\frac{D^{(\text{wb})}(x_I, y_I, z_I)}{D^{(\text{ww})}(x_I, y_I, z_I)} = \exp[-(\mu_{\text{b}} - \mu_{\text{w}})s_2]. \quad (7)$$

For the photon energy considered in our simulations,  $E_0 = 1.25$  MeV, the attenuation coefficients can be calculated easily (see Hubbell and Seltzer, 2004) and one obtains  $\mu_{\text{b}} = 0.11174 \text{ cm}^{-1}$  and  $\mu_{\text{w}} = 0.06323 \text{ cm}^{-1}$ . On the other hand the length  $s_2$  can vary from source to source, depending on the position of the isocenter. If the phantom is centered with respect to the helmet, that is if the isocenter is at  $I[0,0,0]$ ,  $s_2 = 5$  mm for all the sources. In this



case the dose ratio is 0.976, and a reduction of 2.4% is found. This is the minimum reduction found for all positions of the isocenter. By varying them in the interval  $(-70 \text{ mm}, 70 \text{ mm})$  in the three directions, we sample the full volume of the phantom,  $s_2$  ranges between 0.5 cm and 2.7 cm and the reduction due to the bone inhomogeneity varies between 2.4% and 12.2%. These results indicate that, as we have found in our simulations, a few percent reduction in the dose at the isocenter is expected due to the bone inhomogeneity, independently of the position of the isocenter.

The air-tissue interface (central panels) produces a slight increase (1-2% at most) in the dose at the isocenter, in comparison with that found for the homogeneous phantom, when it is situated far from the separation surface. When the interface is approached the relative difference  $\Delta_{\text{ww}}^{(m_1 m_2)}$  increases, the dose at the isocenter for the inhomogeneous phantom is  $\sim 5\%$  larger than that obtained for the homogeneous phantom and this occurs until a point very close to separation surface is reached. Once the isocenter is situated at this position, the dose calculated for the heterogeneous phantom reduces strongly with respect to that of the homogeneous one. This reduction is  $\sim 15\%$  in the inner side and  $\sim 10\%$  in the outer side of the air cube.

A similar situation is observed when both interfaces are present (lower panels) except for a general decrease of the dose at the isocenter whatever  $y_I$  is. This shift toward smaller doses is due, as said before, to the presence of the skull, as we can see clearly in the region  $y_I < 0$ , far from the air interface, which shows a behavior rather similar to that plotted in the upper panels. One should point out the fact that the overdosage observed in the region around  $y_I = 30 \text{ mm}$  for the  $\mathcal{P}_{\text{aw}}$  phantom is largely reduced when, in addition, the bone shell is considered.

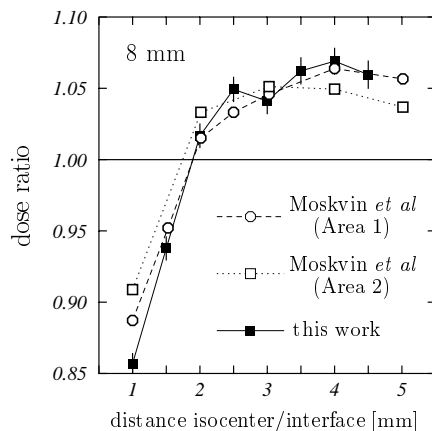


**Figure 5.** Dose ratio at the isocenter for the doses calculated with the  $\mathcal{P}_{\text{aw}}$  and the homogeneous  $\mathcal{P}_{\text{ww}}$  phantoms, as a function of the distance of the isocenter to the air-tissue interface and for the 8 mm helmet. Black squares are our results. Open squares and circles are those of Moskvin *et al* (2004) for two different areas of their phantom.

The results obtained near the air-tissue interfaces can be compared with those found by Moskvin *et al* (2004). In figure 5, we show the dose ratio at the isocenter for the doses calculated with the  $\mathcal{P}_{\text{aw}}$  and the homogeneous  $\mathcal{P}_{\text{ww}}$  phantoms, as a function of the distance of the isocenter to the air-tissue interface. Results correspond to the 8 mm helmet. Black squares are our results. Open squares and circles are those of Moskvin *et al* (2004) for two

different areas of their phantom. As we can see, agreement between the different calculations is rather reasonable.

### 3.4. Effects of the tissue inhomogeneities on dose profiles

The larger effects observed appear when the isocenter is situated nearby an air-tissue heterogeneity. In order to analyze in detail the dose in this situation, we have calculated the quantities  $d_{\text{ww}}^{(m_1 m_2)}(x, y, z)$ , as given by equation (3), for two positions of the isocenter: I[0,34,0] and I[0,66,0]. In these two positions the isocenter is at 1 mm distance from the inner and outer sides of the air cube (region 1), respectively. Some results are plotted in figures 6 and 7.

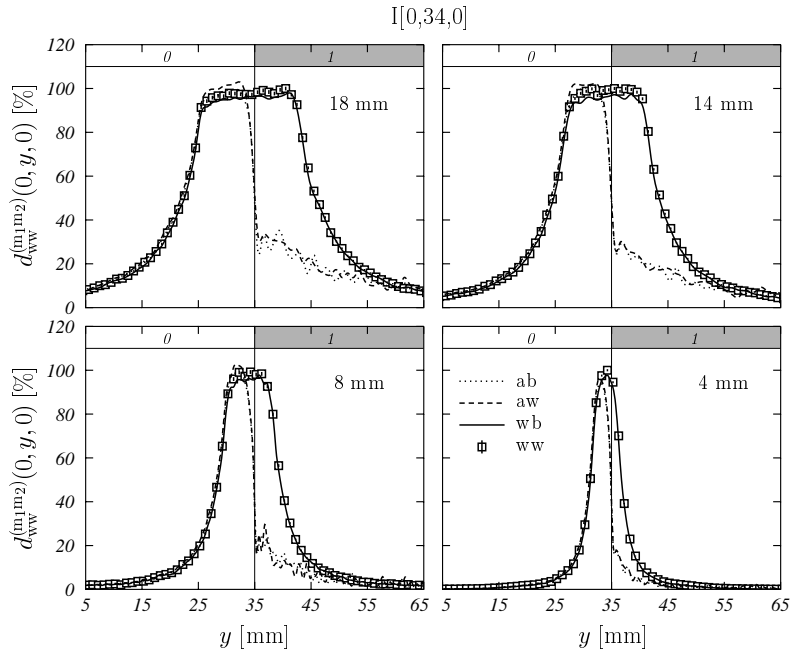


**Figure 6.** Values of  $d_{\text{ww}}^{(m_1 m_2)}(0, y, 0)$  in percentage, as given by equation (3), when the isocenter is situated at I[0,34,0]. The profiles in the  $y$ -axis are shown for the four helmets. The squares correspond to the homogeneous phantom  $\mathcal{P}_{\text{ww}}$ . Solid curves have been obtained with the phantom  $\mathcal{P}_{\text{wb}}$ . Dashed curves represent the results in case of the heterogeneous phantom  $\mathcal{P}_{\text{aw}}$ . Dotted curves take into account the phantom  $\mathcal{P}_{\text{ab}}$ .

Figure 6 shows the profiles along the  $y$ -axis for the four helmets and for the isocenter at I[0,34,0]. Therein the squares correspond to the homogeneous phantom  $\mathcal{P}_{\text{ww}}$ , while solid, dashed and dotted curves have been obtained with the phantoms  $\mathcal{P}_{\text{wb}}$ ,  $\mathcal{P}_{\text{aw}}$  and  $\mathcal{P}_{\text{ab}}$ , respectively. If only the bone is considered (solid curves), a reduction in the plateau region including the maximum dose is observed. This is the same reduction previously discussed for the dose at the isocenter.

On the contrary, the presence of the air-tissue interface (dashed curves) produces a strong reduction of the dose on the “air” side (the right side in this case) of the interface and an enhancement of the dose profile on the “water” side (the left side in this case) of the separation surface. This effects are better seen for the 18 helmet. The main effect of the simultaneous consideration of both interfaces (dotted curves) is to cancel the overdose on

the left side of the interface. The results here obtained are very similar to those plotted in the figure 6 of the work of Moskvin *et al* (2004). These large differences in the dose produced by the air-tissue heterogeneities cannot be neglected.

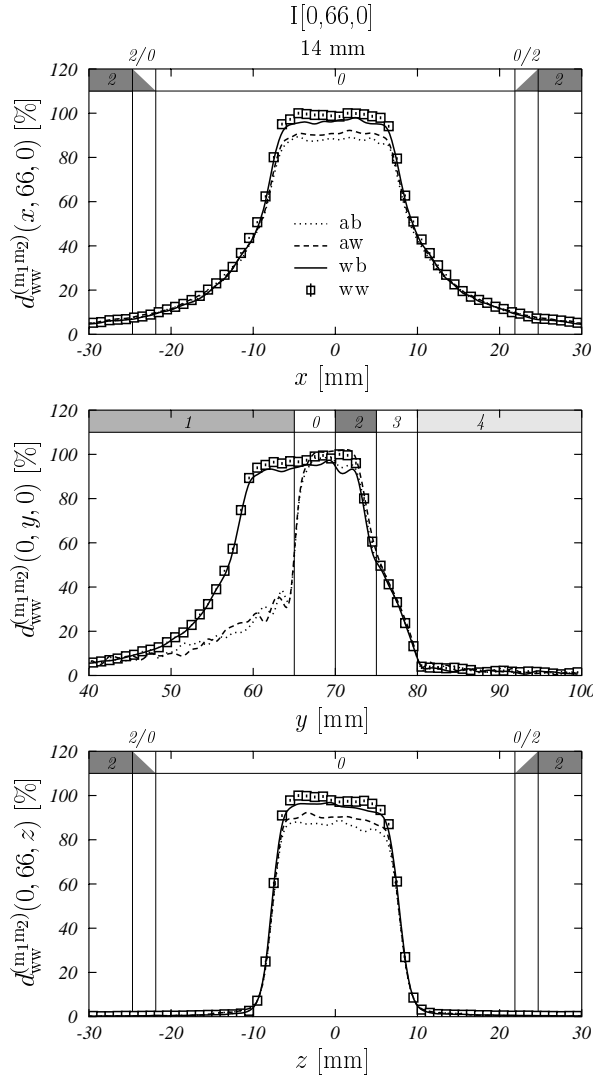


**Figure 7.** Values of  $d_{ww}^{(m_1 m_2)}(x, y, z)$  in percentage, as given by equation (3), when the isocenter is situated at  $I[0,66,0]$ . The profiles in the three cartesian axes are shown for the 14 mm helmet. The lines have the same meaning as in figure 6.

Figure 7 depicts the results obtained for the 14 mm helmet when the isocenter is situated at  $I[0,66,0]$ . The different curves correspond to the same phantoms as in the previous figure. Here the profiles along the three cartesian axes are plotted. Two facts deserve a comment. First, it is appreciable in the upper and lower panels the reduction of the dose produced by the presence of the air-tissue interface (dashed and dotted curves). Also, the comparison between both curves gives us an idea of the additional diminution produced by the bone shell. Second, it is again evident (see medium panel) the strong overdosage produced if the air-tissue interface is not taken into account, but it is also remarkable the reduction in the dose observed in the region 2 when the bone shell is considered (solid curve).

To complete our analysis, we show in figure 8 results similar to those in figure 6 but for

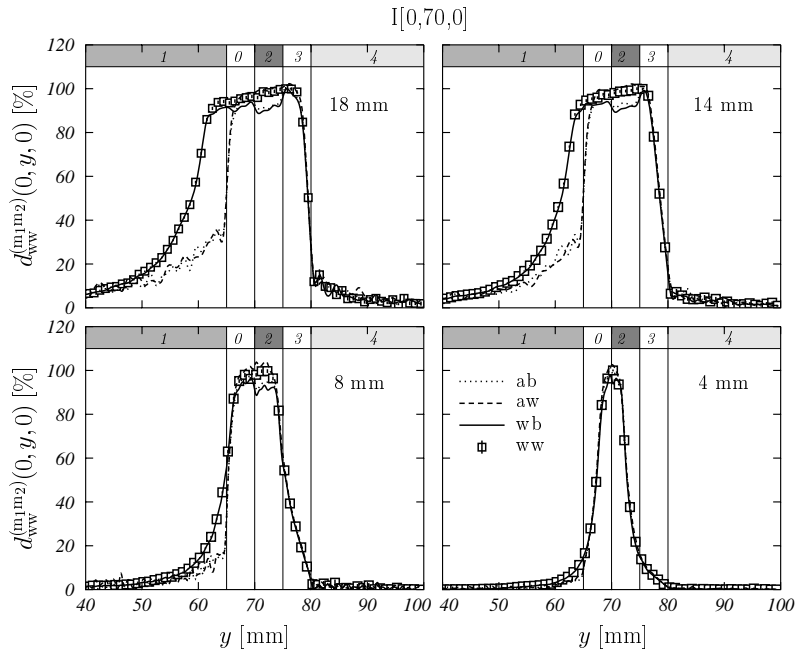


**Figure 8.** Same as in figure 6 but for the isocenter situated at  $I[0,70,0]$ .

the isocenter situated at  $I[0,70,0]$ , that is exactly at the bone-tissue interface. Apart from the reductions observed in the dose nearby the air-tissue interface, here the effect of the bone shell in region 2 is, as expected, stronger than in the previous case.

To finish we point out that, as it is observed in figures 6 and 8 and in the medium panel of figure 7, the dose in the interface air-water is, in all cases,  $\sim 50\%$  of the maximum dose obtained for the homogeneous phantom. This result is into agreement with the findings of Moskvin *et al* (2004).

#### 4. Conclusions

In this work we have investigated the dosimetry of the GK in case of heterogeneous phantoms by considering a simplified source model for the single source channels. Calculations have been done by using the Monte Carlo code PENELOPE (v. 2003) for the configuration including 201 unplugged sources and for different positions of the isocenter of the GK.

The use of the simplified model produces results for the dose profiles at the isocenter which are in agreement with previous calculations done with EGS4, whereas they show discrepancies with the predictions of the GP, mainly at the interfaces.

In general we can say that the presence of typical tissue inhomogeneities produces an underdosage with respect to the results obtained when an homogeneous phantom is considered. This happens for almost all the positions of the isocenter of the GK. This underdosage can reach values larger than 10% in the vicinity of air-tissue interfaces. The only exception of this conclusion occurs when the isocenter is situated at a distance of a few millimeters of the air-tissue separation surface, where an overdosage is produced. However, this overdosage is very small if, in addition to the tissue inhomogeneity, also the bone inhomogeneity is considered.

We have analyzed the doses deposited in phantoms including bone and air inhomogeneities and we have found non-negligible discrepancies with the doses obtained

in case of water homogeneous phantom. In this respect it is worth to mention that an air inhomogeneity simulating the maxillary or frontal sinuses, give rise to large modifications of the dose profiles.

We have found a reasonable agreement with previous calculations performed by Moskvin *et al* with PENELOPE code in the case of the air-tissue interfaces.

In what refers to the bone-tissue inhomogeneity representing the skull, our results show a  $\sim 3\%$  underdosage at the isocenter, with respect to the doses calculated for the homogeneous phantom. This effect can be observed wherever the isocenter is situated.

The discrepancies observed between the results obtained for heterogeneous and homogeneous phantoms suggest that GP predictions must be corrected in order to take care of the air- and bone-tissues inhomogeneities, mainly in those cases in which the interfaces are present nearby the target area.

### Acknowledgments

We kindly acknowledge A. Hamad and H. Mherat for providing us with the GammaPlan predictions quoted in section 3.2. F.M.O. A.-D. acknowledges the A.E.C.I. (Spain), the University of Granada and the I.A.E.A. for funding his research stay in Granada (Spain). E.L.R. acknowledges the University of Granada and the Departamento de Física Moderna for partially funding her stay in Granada (Spain). This work has been supported in part by the Junta de Andalucía (FQM0220).

### References

- Al-Dweri F M O, Lallena A M 2004b A simplified model of the source channel of the Leksell Gamma Knife<sup>®</sup>: testing multisource configurations with PENELOPE *Phys. Med. Biol.* **49** 3441-53
- Al-Dweri F M O, Lallena A M and Vilches M 2004a A simplified model of the source channel of the Leksell GammaKnife<sup>®</sup> tested with PENELOPE *Phys. Med. Biol.* **49** 2687-703
- Berger M J 1968 Energy deposition in water by photons from point isotropic sources MIRD Pamphlet No. 2, *J. Nucl. Med. Suppl.* **1** 17-25
- Cheung J Y C, Yu K N, Yu C P and Ho R T K 2001 Dose distributions at extreme irradiation depths of gamma knife radiosurgery: EGS4 Monte Carlo calculations *Appl. Radiat. Isot.* **54** 461-5
- Elekta 1992 *Leksell Gamma Unit-User's Manual* (Stockholm: Elekta Instruments AB)
- Elekta 1996 *Leksell GammaPlan Instructions for Use for Version 4.0-Target Series* (Geneva: Elekta)
- Hamad A, Mherat H 2005 (private communication)
- Hubbell J H, Seltzer S M 2004 *Tables of X-Ray Mass Attenuation Coefficients and Mass Energy-Absorption Coefficients (version 1.4)* <http://physics.nist.gov/xaamdi> (Gaithersburg: NIST)
- Moskvin V, DesRosiers C, Papiez L, Timmerman R, Randall M and DesRosiers P 2004 Monte Carlo simulation of the Leksell Gamma Knife<sup>®</sup>: II. Effects of heterogeneous versus homogeneous media for stereotactic radiosurgery *Phys. Med. Biol.* **49** 4879-95
- Salvat F, Fernández-Varea J M and Sempau J 2003 *PENELOPE - A code system for Monte Carlo simulation of electron and photon transport* (Paris: NEA-OECD)
- Solberg T D, DeMarco J J, Holly F E, Smathers J B and DeSalles A A F 1998 Monte Carlo treatment planning for stereotactic radiosurgery *Radiother. Oncol.* **49** 73-84
- Wu A 1992 Physics and dosimetry of the gamma knife *Neurosurg. Clin. N. Am.* **3** 35-50
- Wu A, Lindner G, Maitz A, Kalend A, Lunsford L D, Flickinger J C and Bloomer W D 1990 Physics of gamma knife approach on convergent beams in stereotactic radiosurgery *Int. J. Radiat. Oncol. Biol. Phys.* **18**, 941-9
- Yu C and Shepard D 2003 Treatment planning for stereotactic radiosurgery with photon beams *Technol. Cancer. Res. T.* **2** 93-104